Salt Effects on the Amide Hydrogen Exchange of Bovine Pancreatic Trypsin Inhibitor

Morten Christoffersen, Simon Bolvig, and Erik Tüchsen*

Roskilde University, Institute of Life Sciences and Chemistry, P.O. Box 260, DK4000 Roskilde, Denmark

Received July 25, 1995; Revised Manuscript Received November 28, 1995[⊗]

ABSTRACT: Peptide hydrogen exchange is measured in bovine pancreatic trypsin inhibitor (BPTI) by 2D NMR in KCl solutions varying between 0.02 and 0.43 M. The effects of salt are analyzed for 16 assigned peptide groups located near the protein−solvent interface in the crystal structure. Salt effects are obtained for exchange by H^+ and OH^- catalysis, at pH 2.3 and 5.3, respectively. Semilogarithmic plots of rate constants vs the square root of the ionic strengths are virtually linear. The salt effects, taken as the slopes of these plots, vary both in size and sign for each catalytic process, reflecting the variation of local electrostatic field at the exchanging site. The effects are correlated with electrostatic potentials calculated by the finite differences method, taking into account both ionic and dipolar charges in the static structure. This suggests that the transition complexes between the catalyst and the protein are formed with the protein structure very similar to the crystal structure.

Although salt effects on hydrogen exchange (HX)[1] in proteins may provide valuable information about the mechanism of the exchange reaction (Hvidt & Nielsen, 1966), they have only scarcely been investigated. Salt effects are interesting owing to their inherent information about the conformational processes associated with the exchange reaction. In the classical Linderstrøm-Lang model (Scheme 1), the thermal distribution of protein conformations is divided into subsets "C" and "O". "O" contains conformations that are open to exchange of a given peptide group, and "C" contains those that are not (Hvidt & Nielsen, 1966; Woodward & Hilton, 1979, 1980; Barksdale & Rosenberg, 1982; Englander & Kallenbach, 1984; Pedersen et al., 1993):

Scheme 1

$$C \underset{k_2}{\overset{k_1}{\rightleftharpoons}} O \xrightarrow{k_3} X$$

The lack of knowledge concerning the nature of the "O" conformations is the origin of the persistent controversy in hydrogen exchange. The salt effects on HX originate from the salt-dependent polarization of the solution surrounding the protein. The return field from the polarization attenuates the electrostatic contribution to the energy barrier of the exchange reaction. The electrostatic potentials measured by the salt effects, consequently, relate to the transient accessible protein conformation, "O" in Scheme 1.

Older studies, in which the exchange at single sites was not resolved, tended to conclude that effects of salt on HX were small or absent. The best of these studies could conclude that salt effects measure the protein net charge, as predicted by simple Debye-Hückel and "smeared charge" electrostatic theory (Leichtling & Klotz, 1966; Kakuda & Mueller, 1975; Schinkel et al., 1985). Model compound studies have been on a similar level. In charged synthetic homo- or heteropolymers, HX responds strongly to solvent salt, in correlation with the molecular net charge (Kakuda et al., 1971; Kim & Baldwin, 1982). For neutral model compounds, as for some of the investigated proteins, salt effects are vanishingly small (Schleich et al., 1968, 1971) and may not rise above experimental error (Englander & Poulsen, 1969; Kim & Baldwin, 1982). A few single-site salt effects were obtained by NMR for surface peptide groups in BPTI (Tüchsen & Woodward, 1985b, 1987). We include these in our interpretation here.

Salt effects on kinetic processes in macromolecules are expected to depend on the local electrostatic field in the microenvironment where the reaction occurs rather than on the net charge of the macromolecules. A lucent example is the substrate binding to Cu−Zn superoxide dismutase (Cudd & Fridovich, 1982; Getzoff et al., 1983; Allison et al., 1988; Harvey, 1989). In spite of a negative net charge of superoxide dismutase, the effect of salt on its catalytic rate indicates a positive electrostatic environment at the active site. This is ascribed to the local field of the histidine charge in the active cleft of superoxide dismutase.

Methods both for assessing HX by NMR and for computing electric field energies based on the actual shape of the protein (Warwicker & Watson, 1982; Gilson & Honig, 1988) have been vastly improved in recent years. This continued development calls for a reinvestigation of salt effects on protein HX.

The experiments reported in this paper concerns salt effects on HX of peptide groups near the solvent interface of BPTI. Exchange rates were obtained for several partially buried peptide groups at KCl concentrations ranging from 0.02 to 0.43 M. The salt effects show a considerable variation from site to site. This indicates that the HX depends on the local electrostatic field. We find that the salt effects are correlated with calculated electrostatic potentials based on the BPTI crystal structure. We conclude that, for this sample of

* Corresponding author.

⊗ Abstract published in *Advance ACS Abstracts,* February 1, 1996.

[1] Abbreviations: HX, hydrogen exchange; BPTI, bovine pancreatic trypsin inhibitor; COSY, two-dimensional correlation spectroscopy; FID, free induction decay; LP, linear prediction; NMR, nuclear magnetic resonance spectroscopy.

0006-2960/96/0435-2309$12.00/0

Table 1: Sample Composition

no.	C_{KCl}[a]	pH	no.	C_{KCl}[a]	pH
1	0.060	2.16	6	0.018	5.06
2	0.095	2.34	7	0.034	5.28
3	0.145	2.21	8	0.060	5.29
4	0.220	2.24	9	0.097	5.61
5	0.426	2.33	10	0.180	5.57
			11	0.340	5.52

[a] In mol/L.

peptide groups, the catalyst combines with its target sites while the protein conformation is closely similar to the crystal structure.

MATERIALS AND METHODS

BPTI is a gift from Novo-Nordisk A/S, Copenhagen. The protein, five times recrystallized and lyophilized, was dissolved in water, thoroughly dialyzed to remove traces of salt, and lyophilized in aliquots containing 16 mg of BPTI. These were redissolved in 0.5 mL of H_2O (5 mM BPTI) containing 1−400 mM KCl. Adjustment of pH to the experimental value was made by addition of HCl or KOH, and the samples were relyophilized and stored at −20 °C until they were used. An exchange experiment was initiated by dissolving the sample in 0.5 mL of D_2O and transferring to an NMR sample tube immediately before starting the acquisition of the first NMR spectrum. During the course of the experiments, samples were kept in the sealed NMR sample tubes in a water bath at 27 ± 0.5 °C or in the NMR probe at that temperature. Typically 24 absolute intensity COSY NMR spectra were measured at 250 MHz (Bruker AC250), spaced by increasing time intervals over 10 weeks. The size of the time domain spectra was 128 × 512 complex data points; the acquisition time, 65 min. Experimental pHs were measured after the experiment directly in the NMR vials, and salt concentrations were obtained from calibrated conductivity measurements. Reported values of pH are direct readings, calibrated with standard buffers at pH 4.01 and 7.00 (25 °C). The composition of the samples are summarized in Table 1.

Fourier transformation and other processing of NMR data were performed after transfer of the time domain spectra to an INTEL 80486-based computer. After Fourier transformation of unapodized FIDs in the t_2 direction, the spectra were expanded in the t_1 direction from 128 to 512 data points by linear prediction (LP) (Stephenson, 1988; Gesmar et al., 1990) and apodized with a combined squared sine bell and exponential multiplication before the second Fourier transformation. The signal to noise ratio was about 2−4-fold improved by using LP rather than zero-filling, and, importantly, the base-plane was considerably flattened. This dramatically improved the reproducibility of peak volume calculations. The LP algorithm taken from Press et al. (1990), was modified to prevent occasional overflow.

Figure 1 shows the assigned cross peaks for which exchange rates are reported here. The peak volume for each cross peak was determined by summing single data point intensities over an area including the peak. Correction for base-plane offset was made by subtracting an average intensity, obtained from a neighboring area with no peak intensity, from the intensity of each data point. Corrected peak volumes were normalized to the volume of a resolved cross peak between nonexchangeable protons (Thr-32 $H^{\beta}H^{\gamma}$) to eliminate differences between spectra. Exchange rates were calculated by nonlinear maximum-likelihood fitting of experimental peak volumes vs time data to an exponential decay. A robust algorithm (Press et al., 1990) was chosen to prevent adverse effects of occasional deviating peak volumes. The algorithm was designed to minimize the target function s,

$$s = \frac{1}{N}\sum_{i=1}^{N}\ln(1 + d_i^2),\ d_i = A_0 \exp(-kt_i) - A_i \qquad (1)$$

where A_i and t_i are experimental peak volumes and exchange times, and the initial peak volume, A_0, and the rate constant, k, are the fitting parameters. The effect of using a robust method instead of a standard procedure is shown in Figure 2. The robust method does not give a normal standard derivation value, but rather the minimized value of s. Second-order catalytic rate constants $k_H = k/[H^+]$ (pH 2.34) and $k_{OH} = k[H^+]/K_w$ [pH 5.29, $K_w = 10^{-14.85}$ M^2 (Covinton et al., 1966)] were calculated to eliminate the effects of small differences in experimental pH. Rate constants were removed from the data set if they were significantly influenced by both acid and base catalysis, that is, if the experimental pH was closer than 0.5 units from the pH of minimum rate, pH_{min}, for the particular peptide group.

Electrostatic potentials were calculated by numeric integration of the linearized Poisson−Boltzmann equation using the finite differences method (Warwicker & Whatson, 1982; Allison et al., 1988). These calculations were performed on a Silicon Graphics 4D work station. The BPTI crystal form II coordinates were modified by rotating the Gly-56 main chain bonds (to $\phi = 80.8°$ and $\psi = 106.8°$) to bring the C-terminal COOH into salt-bridging distance of the N terminus. The high-occupancy conformation was chosen for the Glu-7 side chain which features an H-bond to Asn-43 main chain NH. The atom coordinates were incorporated in a 45 × 45 × 45 grid with a 1 Å grid spacing. The convergence of the iteration was accelerated by 30% overrelaxation and was complete after ca. 100 steps. To eliminate the effects of the limited grid resolution and short distance to grid edges, potentials were averaged for several calculations (usually 10), with the protein molecule randomly rotated before incorporation in the grid. The dielectric constants were 8 for grid points inside the protein, and 80 elsewhere. A Debye−Hückel screening factor corresponding to 0.1 M salt was used in the space outside the protein. All atoms of the protein were assigned fractional charges by the algorithm of Gasteiger and Marsili (1980). The output of the calculation was potentials with arbitrary units at the sites of each atom of the structure.

RESULTS

HX was followed at pH 2.3 (H^+ catalysis for most NH's) and pH 5.3 (OH^- catalysis), at KCl concentrations ranging from 0.02 to 0.43 M (Table 1). The time schedule for sampling the exchange was optimized for rates in the range 10^{-2}−10^{-4} min^{-1}. Exchange rates spanning $10^{-1.7}$−$10^{-5.2}$ min^{-1} were obtained from the LP expanded COSY spectra (Table 2). The listing in Table 2 includes all residues with resolved NH−C^{α}H cross peaks and exchange rates within that range. Exchange salt dependencies were obtained for

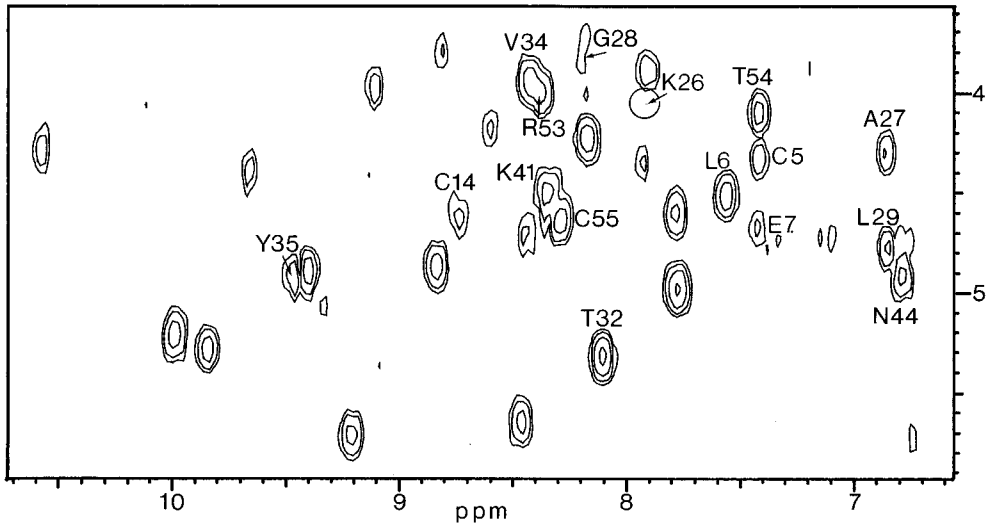

FIGURE 1: Amide region of the 250 MHz absolute-intensity COSY spectrum of BPTI. The locations where the exchange is measured are indicated. The sample contained 5 mM BPTI, pH 1.5, 0.3 M KCl. Thirty-two transients were acquired for 128 t_2 FIDs; there were 512 complex data points. Squared sine wave apodization is applied in both dimensions. The t_1 dimension was expanded to 512 spectra by standard zero-filling. Overlapping NH−C$^{\alpha}$H cross peaks for Val-34/Arg-53, Lys-41/Cys55, Tyr-35/(Phe-22), and Lys-26/(Gly56) were fully resolved in spectra expanded by linear prediction.

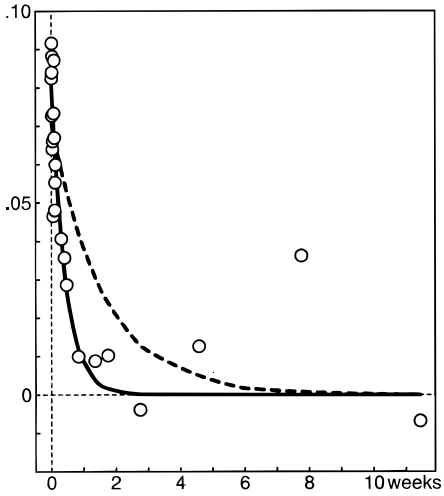

FIGURE 2: Exponential decay of Glu-7 amide proton intensity. The fitted maximum likelihood (solid line) and nonlinear least-squares (dotted line) exponential decay are shown. The vertical axis is the Glu-7 NH−C$^{\alpha}$H cross peak intensity, relative to the constant intensity of the Thr-32 C$^{\beta}$H−C$^{\gamma}$H$_3$ cross peak.

16 of the 54 non-proline peptide groups in BPTI. For 6 of them data were obtained for both catalytic processes. In the crystal structure these peptide groups are typically located near the protein−solvent interface, and all but four of them (Cys-5, Leu-6, Tyr-35, and Asn-44) have some portion of their surface exposed to the solvent. The Tyr-35 peptide group is somewhat atypical for the sample. It is often considered to be a member of the slowly exchanging core of BPTI. Static accessibilities were calculated for the CO and NH moieties of the peptide bonds (Lee & Richards, 1971). These are listed in Table 3.

The Salt Effects. Debye−Hückel plots [log(k) vs $\sqrt{I}$] of the data in Table 2 are shown in Figure 3. The slopes of these plots (B) are used as a measure of the salt effects and are listed in Table 4.

At increasing salt concentration, acid-catalyzed HX is usually accelerated and base-catalyzed HX is slowed. This pattern is the one expected for screening of the electrostatic interactions between catalyst ions and the overall positive field from the BPTI net charge of +11 (pH 2.3) or +6 (pH 5.3). Salt effects previously reported for three acid-catalyzed and five base-catalyzed HX rates (Tüchsen & Woodward, 1985b, 1987) also follow this pattern.

Unlike what is expected from the net charge model, we observe a considerable site-dependent variation of the salt effects. The ratios of exchange rates at 0.02 and 0.43 M salt range from 0.6- to 2.8-fold for acid-catalyzed HX and 0.7- to 9.7-fold for base-catalyzed HX. The salt effects on acid-catalyzed HX of Ala-27 NH and on base-catalyzed HX of Cys-5 NH are virtually zero. Interestingly, one of the effects on acid-catalyzed HX (Glu-7) and three of the effects on base-catalyzed HX (Leu-6, Lys-26, and Arg-53) have their sign reversed, indicating that the transition complexes in these cases are formed in an environment with an electrostatic potential opposite to that formed by the net charge. Such "inverse" salt effects on HX have not been reported previously. The inverse salt effect for Glu-7 at pH 2.3 is particularly interesting since, at that pH, all carboxyl groups are protonated, requiring the negative potential to come from short-range dipolar charges. An experiment was performed at pH 1.5, including three salt concentrations, to verify this finding (data not shown). All salt effects were reproduced, and the experiment, in turn, reconfirmed the H^+ catalysis for Glu-7 at pH $\leq$ 2.3.

Exchange Kinetics. A few previously unpublished acid-catalyzed rate constants and values of pH_{min} are included in the data in Table 4. These are for Cys-5, Glu-7, Leu-29, and Thr-54. A very high pH_{min} of 3.9 is suggested for Leu-29, comparable to that of Ala-16 at pH 4.2 (Tüchsen & Woodward, 1987). High pH_{min} values are expected for peptide groups, like Leu-29 and Ala-16, with exposed carbonyl oxygen and buried NH (Table 3). This pattern is an effect of different steric hindrance for attack of the H^+ and OH^- catalysts on peptide O and NH, respectively. Strong negative electrostatic potential could, in principle, be an alternative explanation. This is ruled out by the finding of salt effects for Leu-29 compatible with a positive electrostatic field at both pH 2.3 and 5.3. Other values of

Table 2: Exchange Rate Constants Obtained from 2D NMR Spectra

	sample									
	1		2		3		4		5	
Cys-5	−3.89[a]	0.40[b]	−4.13	0.77	−4.04	0.32	−3.92	0.13	−3.74	0.15
Leu-6	−3.95	0.10	−3.99	0.14	−3.74	0.08	−3.61	0.15	−3.60	0.07
Glu-7	−3.61	0.36	−3.66	0.52	−3.75	0.20	−3.83	0.65	−3.89	0.51
Cys-14	−4.19	0.29	−4.34	0.61	−4.25	0.61	−4.16	0.86	−4.15	0.41
Ala-27	−2.31	0.05	−2.37	0.07	−2.25	0.07	−2.27	0.10	−2.37	0.04
Gly-28.1	(−3.38	142.4)	−3.45	0.08	−3.29	0.04	−3.33	0.43	−3.39	0.16
Gly-28.2	−3.36	0.05	−3.43	0.06	−3.26	0.06	−3.26	0.06	−3.29	0.05
Leu-29	−4.52	1.51	−4.70	1.25	−4.61	2.36	−4.57	1.61	−4.60	0.44
Thr-32	−3.81	0.03	−3.86	0.02	−3.74	0.01	−3.69	0.01	−3.73	0.06
Val-34	−3.28	0.01	−3.40	0.07	−3.19	0.05	−3.16	0.02	−3.11	0.03
Lys-41	−4.40	0.12	−4.44	0.12	−4.40	0.40	−4.32	0.13	−4.21	0.08
Thr-54	−4.44	0.53			−4.46	0.15	−4.39	0.15		

	sample											
	6		7		8		9		10		11	
Cys-5	−2.78	0.04	−2.58	0.06	−2.52	0.17					−2.35	0.32
Leu-6	−3.39	0.22	−3.10	0.15	−3.02	0.13	−2.96	0.26	−2.75	0.06	−2.83	0.11
Glu-7			−3.95	0.25	−3.86	0.25	−3.55	0.38	−3.64	0.47	−3.79	1.02
Lys-26	−2.28	0.25	−2.00	0.82							−1.71	0.23
Leu-29	−4.59	0.17	−4.42	0.54	−4.40	0.82	−4.11	9.06	−4.32	0.22	−4.31	2.30
Tyr-35	−4.99	2.49	−4.81	1.41	−4.95	0.73	−4.83	1.71	−5.23	1.74	−5.02	1.45
Lys-41	−2.86	0.01					−2.50	0.02	−2.63	0.02	−2.69	0.04
Asn-44	−4.82	0.84	−4.74	1.22	−4.74	0.89	−4.56	0.66	−4.96	4.78	−4.68	1.68
Arg-53	−3.75	0.33	−3.69	0.59	−3.53	0.24	−3.08	0.22	−3.18	0.14	−3.22	0.16
Thr-54	−2.68	0.02	−2.45	0.02	−2.53	0.02	−2.21	0.07	−2.38	0.08		
Cys-55	−3.66	0.08	−3.43	0.12	−3.48	0.07	−3.08	0.07	−3.33	0.13	−3.45	0.22

[a] log(k), where k is the rate of exchange (min^{-1}). [b] Relative error, s/k, where s is the error function defined in eq 1. Data in parantheses are not used.

Table 3: Static Accessibilities and Hydrogen Bonds

	static accessibility[a]		hydrogen bonds[b]	
residue	SA_{NH} (%)	SA_{CO} (%)[c]	NH···	CO···[c]
Cys-5	0	0	+	+
Leu-6	0	0	+	−
Glu-7	0.5	28.0	+	−
Cys-14	0	8.6	-	−
Lys-26	3.0	33.3	+	−
Ala-27	0	32.6	+	−
Gly-28	0	31.0	+	−
Leu-29	0	17.0	−	−
Thr-32	7.6	0	−	+
Val-34	7.9	0	−	+
Tyr-35	0	0	+	−
Lys-41	0	32.7	−	−
Asn-44	0	0	+	−
Arg-53	1.0	1.7	+	+
Thr-54	0	32.6	+	−
Cys-55	0	13.0	+	−

[a] Probe radius, 1.4 Å. Values are relative to the maximum accessible area of the group, obtained by rerunning the calculation with all other atoms removed, except those directly bonded to atoms of the group. [b] Taken from Wlodawer et al. (1987a,b). [c] Carbonyl group of the previous residue in the sequence.

pH_{min} coincide within 0.1 pH units previously published values (Table 4).

The exchange rates from LP expanded 2D NMR (Table 4) compare reasonably with rates previously determined by 1D NMR (Tüchsen & Woodward, 1985a, 1987). The 2−4-fold faster rates obtained here are, in part, explained by the difference in experimental temperature. Larger, 2−10-fold, discrepancies between base-catalyzed rates in Table 4 and those of Wagner and Wüthrich (1982) probably are due to incomplete quenching of the exchange during the 12 h acquisition of NMR spectra in their experiments.

Electrostatic Modeling. The choice of axis transformation to obtain linear plots depends on the electrostatic model used to describe the effects. The log(k) vs square root of the ionic strength, $\sqrt{I}$, linearization is derived from the classical point charge description of small ions. This model appears rather inappropriate for the present system. In the Tanford-Kirkwood model (1957), the zero-order salt-dependent term is $a\kappa/(1 + a\kappa)$, where a is the ion exclusion radius of the spherical "protein" molecule, and κ is the Debye−Hückel screening parameter, proportional to $\sqrt{I}$. Linear plots of log(k) vs $\sqrt{I}$ require $a\kappa$ to be <1, which, for a molecule like BPTI, would occur only at very low ionic strengths. Under the present circumstances, $a\kappa$ is larger than unity. The salt-dependent term should then be approximated by $1 - (1/a\kappa)$, predicting linear plots of log(k) vs $1/\sqrt{I}$. This transformation is also derived from the much simpler Goüy−Chapman model (McLaughlin, 1989). Substituting $\sqrt{I}$ for $1/\sqrt{I}$ in Figure 3, however, results in pronounced curvatures for the majority of the plots. In a study of salt effects on acid dissociation constants in BPTI, Shire et al. (1974a,b) also found the simple Debye−Hückel transformation to be superior to linearizations derived from the Tanford−Kirkwood model.

The correlation of the salt effects with calculated local electrostatic potentials is tested in Figure 4. The electrostatic potentials are obtained from the Poisson−Boltzmann finite differences calculation (Warwicker & Whatson, 1982; Allison et al., 1988) and refer to the BPTI crystal form II structure (Wlodawer et al., 1984). Electrostatic potentials relating to acid-catalyzed rates were calculated with all carboxyl groups protonated, and potentials relating to base-catalyzed rates were calculated with the carboxylic groups

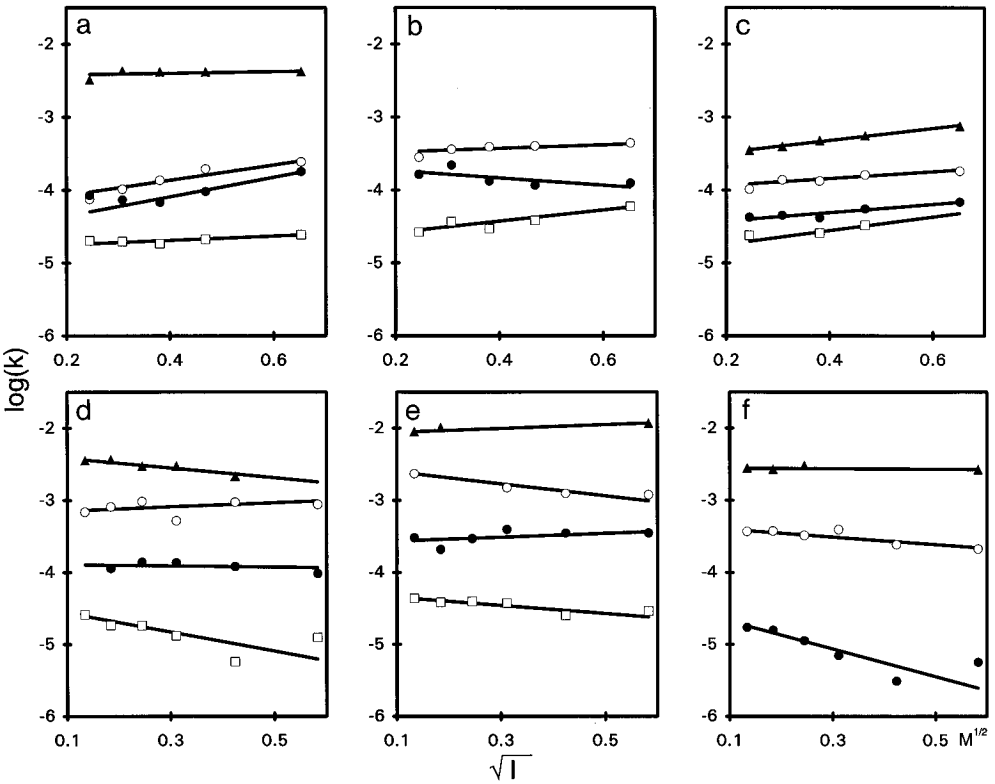

FIGURE 3: Effects of salt concentration on hydrogen exchange rates. Exchange rates are measured at 27 °C and corrected to pH 2.34 (frame a−c) and pH 5.29 (frame d−f). The assignments are (a) ▲, Ala-27; ○, Leu-6; ●, Cys-5; □, Leu-29; (b) ○, Gly-28; ●, Glu-7; □, Lys-41; (c) ▲, Val-34; ○, Thr-32; ●, Cys-14; □, Thr-54; (d) ▲, Thr-54; ○, Leu-6; ●, Glu-7; □, Asn-44; (e) ▲, Lys-26; ○, Lys-41; ●, Arg-53; □, Leu-29; (f) ▲, Cys-5; ○, Cys-55; ●, Tyr-35.

Table 4: Salt Effects on Hydrogen Exchange in BPTI

	acid catalysis		base catalysis			
	k_H ($I = 0$)[a]	B[b]	k_{OH} ($I = 0$)[c]	B[b]	pH_{min}[d]	
Cys-5	5.18	1.33 ± 0.01	10.24	−0.04 ± 0.05	2.9	
Leu-6	11.50	1.04 ± 0.01	2.44	0.28 ± 0.05	3.1	(3.0[e])
Glu-7	50.50	−0.49 ± 0.05	0.47	−0.08 ± 0.02	3.1	
Cys-14	6.33	0.57 ± 0.04				(2.8[f])
Lys-26			30.05	0.26 ± 0.04		(2.5[e])
Ala-27	793.96	0.11 ± 0.06				(3.0[e])
Gly-28	65.22	0.28 ± 0.01				
Leu-29	3.39	0.30 ± 0.01	0.19	−0.57 ± 0.01	3.9	
Thr-32	20.46	0.47 ± 0.01				(2.7[e])
Val-34	49.17	0.82 ± 0.01				(2.8[e])
Tyr-35			0.12	−1.93 ± 0.02		
Lys-41	4.01	0.77 ± 0.01	11.01	−0.84 ± 0.04	3.0	(2.9[f])
Asn-44			0.14	−1.33 ± 0.02		
Arg-53			0.93	0.26 ± 0.02		(3.0[g])
Thr-54	2.55	0.94 ± 0.01	16.27	−0.68 ± 0.01	3.0	
Cys-55			1.62	−0.53 ± 0.03		

[a] Acid-catalyzed rate constant (10^{-3} M^{-1} min^{-1}). [b] Salt effects measured as slopes of the Debye-Hückel plots ($M^{-1/2}$), including standard derivations. [c] Base-catalyzed rate constant (10^6 M^{-1} min^{-1}). [d] $pH_{min} = {}^1/_2[pK_W + \log(k_H/k_{OH})]$ where k_H and k_{OH} refer to 0.3 M salt, $pK_W = 14.85$. [e] Tüchsen and Woodward, 1985a. [f] Tüchsen et al., 1987. [g] Tüchsen and Woodward, 1987.

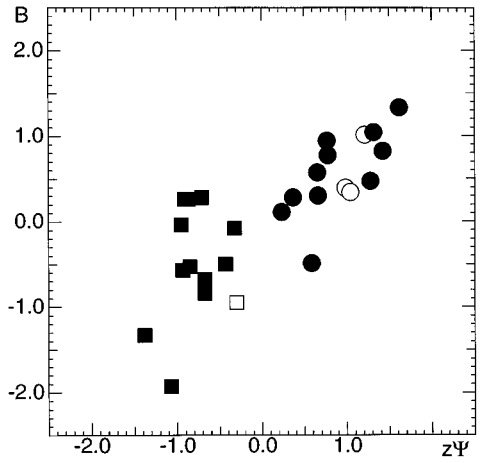

FIGURE 4: Salt effects, B, vs $z\Psi$ where z is the catalyst charge and Ψ is the electrostatic potential calculated for peptide group locations in the crystal form II structure. (●) Acid-catalyzed exchange at pH 2.3; (■) base-catalyzed exchange at pH 5.3. Closed symbols are used for the data from Table 4, open symbols for data from Tüchsen and Woodward (1985, 1987). Calculated potentials are in arbitrary units and are averaged over the atom sites of C, N, and O for acid catalysis and over C, N, and HN sites for base catalysis. A field offset of 0.43 units, due to uneven cancellation of permanent dipoles, is subtracted from calculated potentials. The correlation coefficient for the data from Table 4 is 0.77.

ionized. All atoms were supplied with fractional dipolar charges. Potentials were extracted from the grid and averaged over the sites of C, N, and O for acid catalysis, and over C, N, and HN for base catalysis. Linear regression of the data in Figure 4 provides a correlation coefficient $r = 0.77$ for the combined acid- and base-catalyzed data. Linear regression for the acid-catalyzed data alone gives $r = 0.70$. The correlation is less impressive for the base-catalyzed data: $r = 0.42$. The slopes of the regression lines are identical, within error: 0.65 ± 0.12 for the combined data and 0.8 (±0.3) and 1.0 (±0.7) for acid- and base-catalyzed data, respectively.

Calculated electrostatic energies were somewhat dependent on values chosen for the Debye−Hückel screening factor and the dielectric constant inside the protein, ϵ_p. For the acid-catalyzed data, however, the overall correlation was not seriously affected for ϵ_p varying between 1 and 40, nor by

screening factors corresponding to 0−10 M salt. High ϵ_p and screening factors tended to reproduce better a low electrostatic field near the Glu-7 peptide bond. The correlation for base-catalyzed data could be improved by somewhat unrealistic choices for these parameters. The choice of atomic charges had a considerable effect on the outcome of the calculation. Similarly, slightly altered conformations like those inherent in the 1PIT data file in the Brookhaven Data Bank (Berndt et al., 1993) failed to provide any visible correlation, at least for the first 10 of the entries. The calculation sometimes seems to misfocus the potential wells. For example, in the pH 5.3 calculation, the lowest of all potentials is calculated for the Glu-7 peptide group, while the Leu-6 peptide group is the one showing the inverted salt effect, at that pH.

DISCUSSION

Acid-Catalyzed Exchange. The data presented above provide support for the idea that hydrogen exchange occurs while the protein is in a conformation similar to the time-averaged structure, at least for the acid-catalyzed reaction. The salt effects on the exchange reaction are expected to report the electrostatic potentials experienced by the exchange transition states. The close correlation between salt effects and electrostatic potentials calculated for the crystal structure then indicates that the exchange transition state is well described by the crystal structure. The correlation coefficient, $r = 0.70$, between salt effects on acid-catalyzed exchange and calculated electrostatic potentials could not be expected to be any higher, given the methods applied.

For most of the peptide groups in our data set, this conclusion is well accounted for by the imidic acid mechanism for acid-catalyzed exchange (Perrin, 1989). For 7 of the 11 peptide groups in the data set, the carbonyl oxygen atoms are almost fully embedded in bulk water (Table 3). These can easily combine with H^+ catalyst, without the need for any perturbation of the structure. Clearly, subsequent steps in the exchange event require breakage of NH hydrogen bonds, if present, and a conformational opening to allow solvent access. These steps include the formation of a strong imidic acid, the transfer of imide H to a suitable acceptor, and the reversal of this sequence by attachment of a proton originating from the solvent. If NH forms an H-bond in the time-averaged structure, then the H-bond acceptor might accommodate the imidic proton, initiating an exchange event in a deeply buried peptide group (Tüchsen & Woodward, 1985b). In any case, the breakage of the hydrogen bond and the actual exchange are then secondary events following the protonation of carbonyl O. This mechanism is unlike that in Scheme 1. It could symbolically be written as in Scheme 2:

Scheme 2

$$C \overset{H^+}{\rightleftharpoons} [O] \rightarrow X$$

Base-Catalyzed Exchange. Although the correlation between the salt effects on base-catalyzed exchange and the electrostatic potentials is much less than for acid-catalyzed exchange data, the idea of close proximity of the "O" conformation to the time-averaged structure is still viable for most of the peptide groups. This is especially due to the coinciding slopes of the regression lines through the acid- and base-catalyzed data. The lower correlation, however, can be taken to imply that base-catalyzed exchange requires larger excursions of the protein conformation than does acid-catalyzed exchange. The mechanism for base-catalyzed exchange suggests that a hydroxyl ion removes the peptide H, producing an anion intermediate (Hvidt & Nielsen, 1966). This requires the structure to allow space close to NH for the hydroxyl ion.

Since solvent ionic strength affects all electrostatic interactions in the protein, diminutive conformational changes could occur in response to salt concentration and give rise to complicated additional terms in the salt effects. Such effects, if important, would add to the scatter data in Figure 4. This complication cannot be excluded, although an analysis based on coupling constants in NMR spectra failed to provide evidence for salt-dependent conformational changes. Unfortunately, NMR chemical shifts, which are much more sensitive to subtle structural changes, are not useful in this context, because of their primary electric field dependency. Experiments have shown that the terminal salt bridge in BPTI is unaffected by salt concentrations in the range 0−2 M (unpublished data).

The base-catalyzed salt effects that seem particularly to offend the correlation are the inverse ones. These suggest that the exchange takes place in a perturbed conformation in which electronegative atoms, or a negative charge other than the catalyst ion, is in close proximity to the exchanging peptide NH. The smaller correlation coefficient for base-catalyzed salt effects could well be due to most of the NH groups in the sample being more buried and H-bonded (Table 4).

Buried Amide Groups. While most of the peptide groups of the current data set are in relatively close contact with the surrounding solvent, residues Cys-5, Leu-6, Tyr-35, and Asn-44 are completely buried. The salt effects on acid-catalyzed exchange of Cys-5 and Leu-6, and base-catalyzed exchange of Tyr-35 and Asn-44, are among the largest salt effects observed. They report particularly high positive electrostatic potentials. These potentials are well accounted for by the electrostatic calculation, which in general provides much higher potentials for the low dielectric protein interior than for the exterior regions of the protein. The buried amide groups thereby become strong supporters of the correlation between salt effects and electrostatic effects based on the crystal structure. A similar point was made previously, based on the exchange kinetics of histidine side chains (Bradbury et al., 1980). Perturbed p*K* values for buried histidine side chains in RNAse were found to be reproduced in their C-2 hydrogen exchange kinetics. This shows that the exchange reaction occurs in a conformation similar to crystal structure (Woodward et al., 1982). Our next study will focus on the buried amide protons from the slow-exchange core of BPTI.

Salt effects on acid- and base-catalyzed exchange are expected to report different electrostatic potentials, due to different environments of peptide O and NH target sites for the catalysts. For Cys-5 and Leu-6, this difference is larger than that for other peptide groups in our data set. An additional term for these groups is due to the ionization of the Glu-7 side chain at high pH. The electrostatic calculations do, to a considerable extent, account for these differences for Cys-5 and Leu-6.

Origin of the Salt Effects. A matter of concern for our interpretation is the possibility of hysteresis in establishment

of the electrostatic polarization of the solvent. It is therefore of interest to investigate whether the lifetime of "O" conformations is long enough for solvent polarization to establish itself. The dielectric relaxation rate of the solvent is well known from conductivity measurements (Johri & Roberts, 1990; Kaatze, 1989; von Hippel, 1988; Mashimo et al.,1987; Schmid & Larsen, 1938). A sharp rise in the conductivity at frequencies in excess of 10^9-10^{10} Hz indicates the limit of interest. This frequency coincides with the rotational correlation times for surface water on BPTI (Denisov & Halle, 1995). For the "O" conformation to be sufficiently long lived for dielectric polarization of the solvent to occur, k_2 in Scheme 1 must be less than that limit. Unfortunately, k_2 can be measured only under circumstances where the equilibration between the C and O conformations is rate limiting [i.e., $(k_1 + k_2) < k_3$]. Published values for k_2 under such conditions are in the 1 s^{-1} range at low temperatures and may increase to 10^4 s^{-1} at high temperatures (Woodward & Hilton, 1980; Roder et al., 1984; Pedersen et al., 1993). These conditions are observed for exchange that involve major unfolding/refolding processes.

Under the conditions in the present experiment, however, the pH dependence of k_3 fully penetrates the observed pH profiles (Tüchsen & Woodward, 1985a, 1987), requiring the preequilibrium to be fast [$(k_1 + k_2) \gg k_3$] (Hvidt, 1973). Such (EX2) kinetics may be observed at pHs as high as 11 (Woodward & Hilton, 1980) or higher (Hvidt, 1973). This requires k_2 to be larger than, at least, 10^6 s^{-1}, leaving only 3−4 orders of magnitude for k_2 to vary without jeopardizing the condition of k_2 being less then the water relaxation rate. The consequence of that condition not being filled presumably would be cancellation of the salt effects for "O" conformations that are significantly different from the static structure, in contrast to the observation in Figure 3. Alternatively, if the "O" conformations are like extremes of normal mode fluctuations (Hayward et al., 1993), the bulk solvent might be left relatively unperturbed, and the salt effect might correlate with the electrostatic potentials of the average structure, as observed.

REFERENCES

Allison, S. A., Bacquet, R. J., & McCammon, J. A. (1988) *Biopolymers 27*, 251−269.

Barksdale, A. D., & Rosenberg, A. (1982) *Methods Biochem. Anal. 28*, 1−113.

Berndt, K. D., Güntert, P., Orbons, L. P. M., & Wüthrich, K. (1993) *J. Mol. Biol. 227*, 757−775.

Bradbury, J., Chapman, B., Crompton, M., Norton, R., & Teh, J. (1980) *J. Chem. Soc., Perkin Trans. 2*, 693−699.

Covinton, A. K., Robinson, R. A., & Bates, R. G. (1966) *J. Phys. Chem. 70*, 3820−3824.

Cudd, A., & Fridovich, I. (1982) *J. Biol. Chem. 257*, 11443−11447.

Denisov, V. P., & Halle, B. (1995) *J. Mol. Biol. 245*, 682−697.

Englander, S. W., & Kallenbach, N. R. (1984) *Q. Rev. Biophys. 16*, 521−655.

Englander, S. W., & Poulsen, A. (1969) *Biopolymers 7*, 379−393.

Gasteiger, J., & Marsili, M. (1980) *Tetrahedron 36*, 3219−3228.

Gesmar, H., Led, J. J., & Abildgaard, F. (1990) *Prog. Nucl. Mag. Reson. Spectrosc. 22*, 255−288.

Getzoff, E. D., Tainer, J. A., Weiner, P. K., Kollman, P. A., Richardson, J. S., & Richardson, D. C. (1983) *Nature 306*, 287−290.

Gilson, M. K., & Honig, B. (1988) *J. Comput. Chem. 9*, 327−335.

Harvey, S. C. (1989) *Proteins 5*, 78−92.

Hayward, A., Kitao, A., & Go, N. (1993) *Protein Sci. 3*, 936−943.

Hvidt, Aa. (1973) in *Dynamic Aspects of Conformation Changes in Biological Macromolecules* (Sandron, C., Ed.) pp 103−115, D. Reidel, Dordrecht, The Netherlands.

Hvidt, Aa., & Nielsen, S. O. (1966) *Adv. Protein Chem. 21*, 287−386.

Johri, G. K., & Roberts, J. A. (1990) *J. Phys. Chem. 94*, 7386−7391.

Kaatze, U. (1989) *J. Chem. Eng. Data 34*, 371−374.

Kakuda, Y., & Mueller, D. (1975) *Arch. Biochem. Biophys. 171*, 586−596.

Kakuda, Y., Perry, N., & Mueller, D. D. (1971) *J. Am. Chem. Soc. 93*, 5992−5998.

Kim, P., & Baldwin, R. L. (1982) *Biochemistry 21*, 1−5.

Lee, B., & Richards, F. (1971) *J. Mol. Biol. 55*, 379−400.

Leichtling, B. H., & Klotz, I. M. (1966) *Biochemistry 5*, 4026−4027.

Mashimo, S., Kuwabara, S., Yagihara, S., & Higasi, K. (1987) *J. Phys Chem. 91*, 6337−6338.

McLaughlin, S. (1989) *Annu. Rev. Biophys. Biophys. Chem. 18*, 113−136.

Pedersen, T. G., Thomsen, N. K., Andersen, K. V., Madsen, J. C., & Poulsen, F. M. (1993) *J. Mol. Biol. 230*, 651−660.

Perrin, C. (1989) *Acc. Chem. Res. 22*, 268−275.

Press, W. H., Flannery, B. P., Teukolsky, S. A., & Vetterling, W. T. (1990) *Numerical Recipes in Pascal*: *The Art of Scientific Computing*, Cambridge University Press, New York.

Roder, H., Wagner, G., & Wüthrich, K. (1984) *Biochemistry 24*, 7396−7407.

Schinkel, J. E., Downer, N. W., & Rupley, J. A. (1985) *Biochemistry 24*, 352−366.

Schleich, T., Gentzler, R., & von Hippel, P. H. (1968) *J. Am. Chem. Soc. 90*, 5954−5960.

Schleich, T., Rollefsen, B., & von Hippel, P. H. (1971) *J. Am. Chem. Soc. 93*, 7070−7074.

Schmid, G., & Larsen, E. E. (1938) *Z. Electrochem. Angew. Phys. Chem. 44*, 651−653.

Shire, S. J., Hanania, G. I. H., & Gurd, F. R. N. (1974a) *Biochemistry 13*, 2967−2974.

Shire, S. J., Hanania, G. I. H., & Gurd, F. R. N. (1974b) *Biochemistry 13*, 2974−2979.

Stephenson, D. S. (1988) *Prog. Nucl. Mag. Reson. Spectrosc. 20*, 515−626.

Tanford, C., & Kirkwood, J. G. (1957) *J. Am. Chem. Soc. 20*, 5333−5339.

Tüchsen, E., & Woodward, C. (1985a) *J. Mol. Biol. 185*, 405−419.

Tüchsen, E., & Woodward, C. (1985b) *J. Mol. Biol. 185*, 421−430.

Tüchsen, E., & Woodward, C. (1987) *J. Mol. Biol. 193*, 793−802.

Tüchsen, E., Hayes, J. M., Ramaprasad, S., Copie, V., & Woodward, C. (1987) *Biochemistry 26*, 5163−5172.

von Hippel, A. (1988) *IEEE Trans. Electr. Insul. 23*, 801−816.

Wagner, G., & Wüthrich, K. (1982) *J. Mol. Biol. 160*, 343−361.

Warwicker, J., & Watson, H. C. (1982) *J. Mol. Biol. 157*, 671−679.

Wlodawer, A., Walter, J., Huber, R., & Sjölin, L. (1984) *J. Mol. Biol. 180*, 301−329.

Wlodawer, A., Deisenhofer, J., & Huber, R. (1987a) *J. Mol. Biol. 193*, 145−156.

Wlodawer, A., Nachman, J., Gilliard, G. L., Gallagher, W., & Woodward, C. (1987b) *J. Mol. Biol. 198*, 469−480.

Woodward, C. K., & Hilton, B. D. (1979) *Annu. Rev. Biophys. Bioeng. 8*, 99−127.

Woodward, C. K., & Hilton, B. D. (1980) *Biophys. J. 32*, 561−572.

Woodward, C., Simon, I., & Tüchsen, E. (1982) *Mol. Cell. Biol. 48*, 135−160.

BI951711Q